Received: 7 December 2022 | Revised: 27 January 2024 | Accepted: 29 January 2024

DOI: 10.1002/hbm.26624

RESEARCH ARTICLE

WILEY

Compressed cerebellar functional connectome hierarchy in spinocerebellar ataxia type 3

Xinyuan Liu[1,2,3] | Jing Guo[2,3,4] | Zhouyu Jiang[2,3] | Xingli Liu[2,3] | Hui Chen[1] | Yuhan Zhang[1] | Jian Wang[1] | Chen Liu[1] | Qing Gao[3,5] | Huafu Chen[1,2,3,4]

[1]Department of Radiology, Southwest Hospital, Army Medical University (Third Military Medical University), Chongqing, China

[2]School of Life Science and Technology, University of Electronic Science and Technology of China, Chengdu, China

[3]MOE Key Lab for Neuroinformation, High-Field Magnetic Resonance Brain Imaging Key Laboratory of Sichuan Province, University of Electronic Science and Technology of China, Chengdu, China

[4]The Center of Psychosomatic Medicine, Sichuan Provincial Center for Mental Health, Sichuan Provincial People's Hospital, University of Electronic Science and Technology of China, Chengdu, China

[5]School of Mathematical Sciences, University of Electronic Science and Technology of China, Chengdu, China

Correspondence
Huafu Chen, Department of Radiology, Southwest Hosptial, Army Medical University (Third Military Medical University), Chongqing, 400038, China; School of Life Science and Technology, University of Electronic Science and Technology of China, Chengdu, 610054, China.
Email: chenhf@uestc.edu.cn

Qing Gao, School of Mathematical Sciences, University of Electronic Science and Technology of China, Chengdu, 611731, China.
Email: gaoqing@uestc.edu.cn

Chen Liu and Jian Wang, Department of Radiology, Southwest Hospital, Army Medical University (Third Military Medical University), Chongqing, 400038, China.
Email: cqliuchen@foxmail.com and wangjian_811@yahoo.com

Funding information
National Science and Technology Major Project, Grant/Award Number: 2021ZD0201701; Natural Science Foundation of China, Grant/Award Numbers: 81601478, 82071910, 62173070, 82121003, 62036003, 62333003; Senior Medical Talents Program of Chongqing for Young and Middle-aged, Grant/Award Number: 414Z395; University of Electronic Science and Technology of China, Grant/Award Number: ZYGX2021YGLH201;

Abstract

Spinocerebellar ataxia type 3 (SCA3) is an inherited movement disorder characterized by a progressive decline in motor coordination. Despite the extensive functional connectivity (FC) alterations reported in previous SCA3 studies in the cerebellum and cerebellar-cerebral pathways, the influence of these FC disturbances on the hierarchical organization of cerebellar functional regions remains unclear. Here, we compared 35 SCA3 patients with 48 age- and sex-matched healthy controls using a combination of voxel-based morphometry and resting-state functional magnetic resonance imaging to investigate whether cerebellar hierarchical organization is altered in SCA3. Utilizing connectome gradients, we identified the gradient axis of cerebellar hierarchical organization, spanning sensorimotor to transmodal (task-unfocused) regions. Compared to healthy controls, SCA3 patients showed a compressed hierarchical organization in the cerebellum at both voxel-level ($p < .05$, TFCE corrected) and network-level ($p < .05$, FDR corrected). This pattern was observed in both intra-cerebellar and cerebellar-cerebral gradients. We observed that decreased intra-cerebellar gradient scores in bilateral Crus I/II both negatively correlated with SARA scores (left/right Crus I/II: $r = -.48/-.50$, $p = .04/.04$, FDR corrected), while increased cerebellar-cerebral gradients scores in the vermis showed a positive correlation with disease duration ($r = .48$, $p = .04$, FDR corrected). Control analyses of cerebellar gray matter atrophy revealed that gradient alterations were associated with cerebellar volume loss. Further FC analysis showed increased functional connectivity in both unimodal and transmodal areas, potentially supporting the disrupted cerebellar functional

Xinyuan Liu and Jing Guo have contributed equally to this work.

Innovation Team and Talents Cultivation Program of National Administration of Traditional Chinese Medicine, Grant/Award Number: ZYYCXTD-D-202003

hierarchy uncovered by the gradients. Our findings provide novel evidence regarding alterations in the cerebellar functional hierarchy in SCA3.

KEYWORDS
cerebellum, connectome gradient, hierarchical organization, spinocerebellar ataxia type 3

1 | INTRODUCTION

Spinocerebellar ataxia type 3 (SCA3) is a heterogeneous category of inherited progressive neurodegenerative disorders characterized by cerebellar ataxia (Klockgether et al., 2019). Typical symptoms encompass impaired motor coordination and a loss of balance (Rub et al., 2013; Stefanescu et al., 2015). Numerous investigations have consistently demonstrated the importance of cerebellar dysfunction in the pathogenesis of SCA3 (Wan et al., 2020). The cerebellum exhibits diverse afferent and efferent connections with extracerebellar structures, thereby contributing to distinct functional networks related to high-order functions beyond motor control (Guell & Schmahmann, 2020; Olivito et al., 2017; Witter & De Zeeuw, 2015). Critically, the presence of cerebellar damage is linked to motor, cognitive, and emotional impairments, which are associated with alterations in intra-cerebellar and cerebellar-cerebral pathways (O'Callaghan et al., 2016; Tzvi et al., 2017; Zhang et al., 2020).

Previous studies employing seed-based analysis or network-based analysis have demonstrated disrupted functional connectivity between brain regions in other types of SCAs, such as SCA2 (Cocozza et al., 2015; Olivito et al., 2017), SCA7 (Hernandez-Castillo et al., 2013; Hernandez-Castillo et al., 2014), SCA17 (Reetz et al., 2012), suggesting that disease-related deficits may arise from the involvement of distinct functional networks or the specific impairment of certain brain regions due to cerebellar dysfunction. Global functional network reconfiguration has been found in SCA3, with the number of hub nodes decreasing in cognitive areas and increasing in motor-related areas (Chen et al., 2022). Although previous neuroimaging research has contributed to understanding the reorganization of functional systems in SCA3, knowledge of the cerebellar functional hierarchy guided by the continuous spatial architecture of macroscale networks remains unclear and rarely investigated (Bayrak et al., 2019; Huntenburg et al., 2018; Meng et al., 2021).

The proposal of connectome gradient is instrumental for exploring spatial arrangement between distributed functional systems. It expresses high-dimensional resting-state functional connectivity patterns in a continuous, low-dimensional space using a non-linear decomposition approach (Coifman et al., 2005; Margulies et al., 2016). These connectome gradients capture new information regarding how different functional systems of the human brain organize to integrate sensory signals into more abstract representations (Bernhardt et al., 2022; Huntenburg et al., 2018). Notably, the principal gradients have been applied to reveal a functional hierarchy from unimodal regions to transmodal regions of the cerebral cortex and cerebellum in a large group of healthy individuals (Guell et al., 2018; Margulies et al., 2016). Moreover, functional gradients have been successfully employed in the studies of psychiatric and neurological disorders. For example, the whole connectome was gradually affected by ischemic stroke in specific functional gradients (Bayrak et al., 2019) and specific alteration patterns of the extended or compressed principal gradient were associated with widespread deficits observed in autism (Hong et al., 2019), genetic generalized epilepsy (Meng et al., 2021) and schizophrenia (Dong et al., 2020). These studies collectively suggested that connectome gradient could provide a novel view for elucidating the relationship between gradient patterns under pathological perturbations and the widespread deficits observed in diseases. In addition, previous SCAs studies have reported that the volume loss may at least in part explain the cerebellar-related functional connectivity abnormalities (Cocozza et al., 2015; Guo et al., 2023; Hernandez-Castillo et al., 2014). Nevertheless, the impact of pathological perturbations in the cerebellum, known to affect functional connectivity in SCA3 patients, on these connectome gradients and its associations with morphometry changes and clinical scores remains unexplored.

In this study, we utilized connectome gradient to characterize cerebellar hierarchical anomalies in patients with SCA3 compared to HCs at both the network and voxel levels. We further explored functional connectivity changes and potential correlations between altered gradients and clinical severity in brain regions displaying aberrant gradients, aiming to advance our understanding of the relationship between behavioral deficits and gradient alterations in SCA3. The same analytical steps were used to calculate functional gradients for both intra-cerebellar and cerebellar-cerebral functional connectomes. Moreover, we conducted a validation of the impact of gray matter atrophy on the results obtained from the between-group gradient comparison. Based on previous studies (Pereira et al., 2017; Stefanescu et al., 2015; Wan et al., 2020), we hypothesized that SCA3 patients would show altered gradient patterns within the cerebellum and in cerebellar-cerebral circuits compared to HCs. We anticipated that the alterations in connectome gradients in SCA3 patients might be partly explained by gray matter volume (GMV) changes in the cerebellum and would be associated with increased clinical severity.

2 | METHODS

2.1 | Subjects

Forty-five SCA3 patients and 49 age- and gender-matched healthy controls (HCs) with no history of neurological or psychiatric disorders were included in the analysis. These participants were recruited from the First Affiliation Hospital of Army Medical University. The inclusion

criteria for patients with SCA3 were as follows: (1) presented clinical symptoms of SCA3 and passed the genetic test for CAG expansion; (2) didn't receive medical treatment; and (3) didn't have any other genetic disease. All participants gave written informed consent. The neurological motor functions of patients were assessed by an experienced movement disorders neurologist using the Scale for Assessment and Rating of Ataxia (SARA). All procedures involving human participants were approved by the local ethics committee at First Affiliation Hospital of Army Medical University Review Board.

2.2 | MRI data acquisition

Structural and functional MRI scans were acquired using a 3.0T scanner (Siemens Tim Trio, Germany) equipped with the standard Siemens 12-channel head coil in the First Affiliated Hospital of Army Medical University. During the entire scanning acquisition, all participants were instructed to lay still in the supine with closed eyes but stay awake. Functional images were obtained using an echo-planar imaging (EPI) sequence. The scanning parameters were as follows: repetition time = 2000 ms, echo time = 30 ms, field of view (FOV) = 240 × 240 mm^2, matrix size = 64 × 64, voxel size = 3 × 3 × 3 mm^3, 36 transverse slices, 240 volumes, and flip angle = 90°. We acquired a high-resolution structural T1-weighted (T1w) image using a 3D magnetization-prepared rapid gradient-echo pulse sequence (repetition time = 1900 ms, echo time = 2.52 ms, flip angle = 9°, inversion time = 900 ms, FOV = 256 × 256 mm^2; slice thickness = 1 mm, 176 slices, and voxel size = 1 × 1 × 1 mm^3).

2.3 | Image preprocessing

The functional MRI data were preprocessed using Data Processing & Analysis of Brain Imaging software (www.rfmri.org/dpabi, DPABI version 4.3) (Yan et al., 2016) and Matlab scripts. Preprocessing steps included the following: (1) removing the first 10 volumes to ensure image quality (remaining 230 volumes); (2) slice timing corrected to the first slice; (3) realigned; (4) normalizing into the MNI space at a 3 mm isotropic voxel resolution; (5) smoothening using a 6-mm full-width at half-maximum Gaussian kernel; (6) wavelet despiking to remove head motion artifacts (Patel et al., 2014); (7) regressing out nuisance covariates, including 24 head motion parameters, linear trend, white matter signals, cerebrospinal fluid signals; and (8) temporally band-pass filtering at a frequency band of 0.01–0.1 Hz. The analysis was restricted to right-handed subjects due to the influence of handedness on functional connectivity. Three SCA3 patients and one healthy control were excluded due to left-handedness. Additionally, four patients with SCA3 were excluded due to insufficient brain coverage and two SCA3 patients were excluded because their head maximum displacement exceeded 2.0 mm, and their mean framewise displacement (FD) exceeded 0.5 mm (Jenkinson et al., 2002). The final sample consisted of 35 patients with SCA3 and 48 healthy controls. Because the patients with SCA3 showed more head movement than HCs (Mann–Whitney U test: $U = 653$, $p = 0.02$), the mean FD was added as a nuisance covariate in group analysis to further minimize the residual effects of motion (Power et al., 2013; Yan et al., 2013). Global signal regression (GSR) was not performed, as it would alter the distribution of the correlation coefficients and force an increase in negative correlations (Hahamy et al., 2014; Saad et al., 2012).

2.4 | Volume analysis of gray matter

To examine the GMV changes in patients with SCA3, Computational Anatomy Toolbox (https://neuro-jena.github.io/cat//index.html#DOWNLOAD, CAT12 version 12.5) (Gaser et al., 2022) along with the Spatially Unbiased Infratentorial Template (http://www.diedrichsenlab.org/imaging/suit.htm, SUIT) (Diedrichsen, 2006) were employed to process structural data, enabling the evaluation of both whole-brain GMV and cerebellar GMV (cGMV). In each participant, high-spatial-resolution T1-weighted images underwent manual reorientation with the origin placed at the anterior commissure. Subsequently, the T1 images were segmented into gray matter, white matter, and cerebrospinal fluid using CAT12. These tissue segments were then spatially registered to a standard space using the Geodesic Shooting (Ashburner & Friston, 2011). Modulation was performed on the normalized images to adjust for volume changes due to the registration. Total intracranial volume was estimated based on tissue segmentation (Gaser et al., 2022). After CAT12 processing and visual inspection, whole-brain GMV was extracted for each participant. For cerebellar volumetric quantification, we used the SUIT to investigate cerebellar structural changes in SCA3. The cerebellum was first isolated from the surrounding tissue and further segmented into different tissue types (gray matter, white matter, and cerebrospinal fluid) using a probabilistic segmentation algorithm (Ashburner & Friston, 2005). The default probability threshold for the cerebellar isolation map was set at 0.2. Following isolation and segmentation, the cropped images were normalized using Diffeomorphic Anatomical Registration using Exponentiated Lie algebra (DARTEL). These images were then resliced into SUIT space, incorporating Jacobian modulation to ensure that the value of each voxel retained proportionate to its original volume. To get detailed volume information within the cerebellum, the atlas was transformed back into native space of each participant, enabling the quantification of the number of voxels (volume elements) within specific cerebellar lobules. Ultimately, the number of voxels corresponding to cerebellar gray matter was calculated for each participant. All segmented results underwent visual inspection. The whole-brain GMV and cGMV (as estimated using the number of voxels in cerebellar gray matter) were statistically compared between the SCA3 and HC groups using two-sample t-tests, with TIV, age, and gender set as covariates. In addition, the whole-brain GMV and cGMV were considered crucial covariates in subsequent gradient comparisons to analyze the interaction between functional and structural changes.

2.5 | Connectome gradient analysis

Intra-cerebellar and cerebellar-cerebellar connectome gradients were obtained for each subject using the BrainSpace Toolbox (Vos de Wael

et al., 2020). Individual functional connectivity matrices were generated by calculating the Pearson correlation for each subject's time-series matrix. To localize the cerebellum and the cerebrum, the cerebellar template of automated anatomical parcellation AAL3 and cortical Schaefer atlas were used to define their spatial extent, respectively. The thresholded temporal signal-to-noise ratio (TSNR) was applied to exclude spurious voxels and generate a group-level brain mask. Specifically, voxel-wise TSNR was calculated using functions from the BRANT toolbox, with the threshold set to 30 (Xu et al., 2018). The resulting cerebellar template (6517 voxels) and cerebral template (36,914 voxels) were used to characterize functional connectomes for each individual. Correlation matrices (intra-cerebellar: 6517 × 6517; cerebellar-cerebral: 6517 × 36,914) were obtained for each subject to characterize intra-cerebellar and cerebellar-cerebral functional connectomes. To capture the similarity of connectivity patterns across voxels, we thresholded the matrix, retaining only the top 10% of connections in each row, and then computed the cosine similarity matrix (Dong et al., 2020; Margulies et al., 2016). We applied diffusion map embedding, a non-linear manifold learning method, to identify the gradient components that explain the connectome variance (Coifman et al., 2005; Margulies et al., 2016). This method generated a low-dimensional embedding from the high-dimensional functional connectomes. In the embedding space, pairs of voxels showing high similarity in functional connectivity patterns were closer together, whereas voxels with few or no interconnections were further apart. It is worth noting that the algorithm is controlled by two parameters α and t. α controls the effect of the density of sampling points on the stream shape ($\alpha = 0$, maximum effect; $\alpha = 1$, no effect) and t controls the scale of the eigenvalues that control the diffusion operator. In this study, we followed previous advice and set $\alpha = 0.5$ and $t = 0$. This choice preserved the global relationships between data points in the embedded space (Guell et al., 2018; Hong et al., 2019; Margulies et al., 2016; Meng et al., 2021; Vos de Wael et al., 2018). Procrustes rotations were performed to align each subject's gradient components to a group-averaged template derived from all participants to compare gradients between SCA3 and HC groups (Langs et al., 2015).

In accordance with previous studies (Dong et al., 2020; Guell et al., 2018), our analysis solely focused on the first gradient component. The first gradient (or principal gradient) accounted for the majority of data variability and unveiled functional axes spanning from sensorimotor to transcortical functions within the cerebellum and cerebellar-cerebral functional hierarchy. However, it is worth noting that gradient 2 failed to demonstrate replicability at the individual level in the cerebellum.

In accordance with previous studies (Dong et al., 2020; Guell et al., 2018), our analysis solely focused on the first gradient component. The first gradient (or principal gradient) explained the most data variation and revealed sensorimotor-to-transmodal functional axes within the cerebellum and cerebellar-cerebral functional hierarchy. However, it is worth noting that gradient 2 failed to demonstrate replicability at the individual level in the cerebellum (Guell et al., 2018). To demonstrate system-level macroscale hierarchical alterations, the principal gradient was mapped back to the cerebellum (Figure 1a).

2.6 | Statistical analysis

For the demographic data, the statistical software Prism (GraphPad, USA) was used for group comparisons. Age differences were assessed using two-sample *t*-tests, while gender was tested with the Chi-square test. The Mann–Whitney *U* test was used to examine the mean FD. The $p < .05$ was set as significant for all tests. Table 1 shows the demographic data for both SCA3 patients and HCs.

Differences in gradient scores between the SCA3 and HC groups were evaluated at both the network and voxel levels. For network-level comparisons, we utilized a well-established cerebellar seven-network parcellation to summarize the connectome gradient within different functional networks (Buckner et al., 2011). Two-sample t-tests were used to compare gradient scores between the SCA3 and HC groups in each functional network, with age, gender, and FD regressed out. Only FDR-corrected networks ($p < .05$) were considered significant. Voxel-level comparisons were conducted using two-sample t-tests. Age, gender, and FD were set as covariates. Considering that the calculation of intra-cerebellar gradient was based on the cerebellar-cerebral functional connectome, the whole-brain GMV was added as a covariate in the comparison between groups. To account for the influence of cerebellar structural degeneration on functional connectome, we thus reanalyzed the between-group differences of principal gradients after correcting for cGMV as a covariate. Significant differences were reported using the threshold-free cluster enhancement (TFCE) for multiple comparison corrections (10,000 permutations) (Chen et al., 2018). FWE correction was utilized to correct voxel-level findings of gradient comparisons ($p < .05$). Despite surviving the stringent FWE correction, extremely tiny clusters were excluded with a threshold of 10 voxels for gradient comparing findings. Pearson correlation was used to associate the altered voxel-level gradient scores in abnormal brain regions to SCA3 symptom severity. The averaged gradient scores were extracted from brain regions with altered gradients in SCA3 relative to HCs. The statistical analysis workflow is depicted schematically in Figure 1b.

2.7 | Functional connectivity analysis based on clusters of gradient findings

Post-hoc functional connectivity analysis was conducted to investigate the association between the compressed spatial gradient pattern and functional connectivity. Based on the result of voxel-level gradients comparing findings between SCA3 and HCs, clusters surviving in multiple comparison corrections were combined if they had similar anatomical positions in the cerebellum in intra-cerebellar and cerebellar-cerebral gradients comparisons, respectively. Then, these clusters were used to calculate Pearson correlations with every voxel in the cerebellum and cerebral cortex. Subsequently, the correlation coefficients for each FC map were Fisher z-transformed. The statistical analysis was performed between the SCA3 and HC groups using two-sample t-tests, with age, gender, FD, whole-brain GMV, and cGMV included as covariates. Significant differences were reported using TFCE correction (10,000 permutations, $p < .05$).

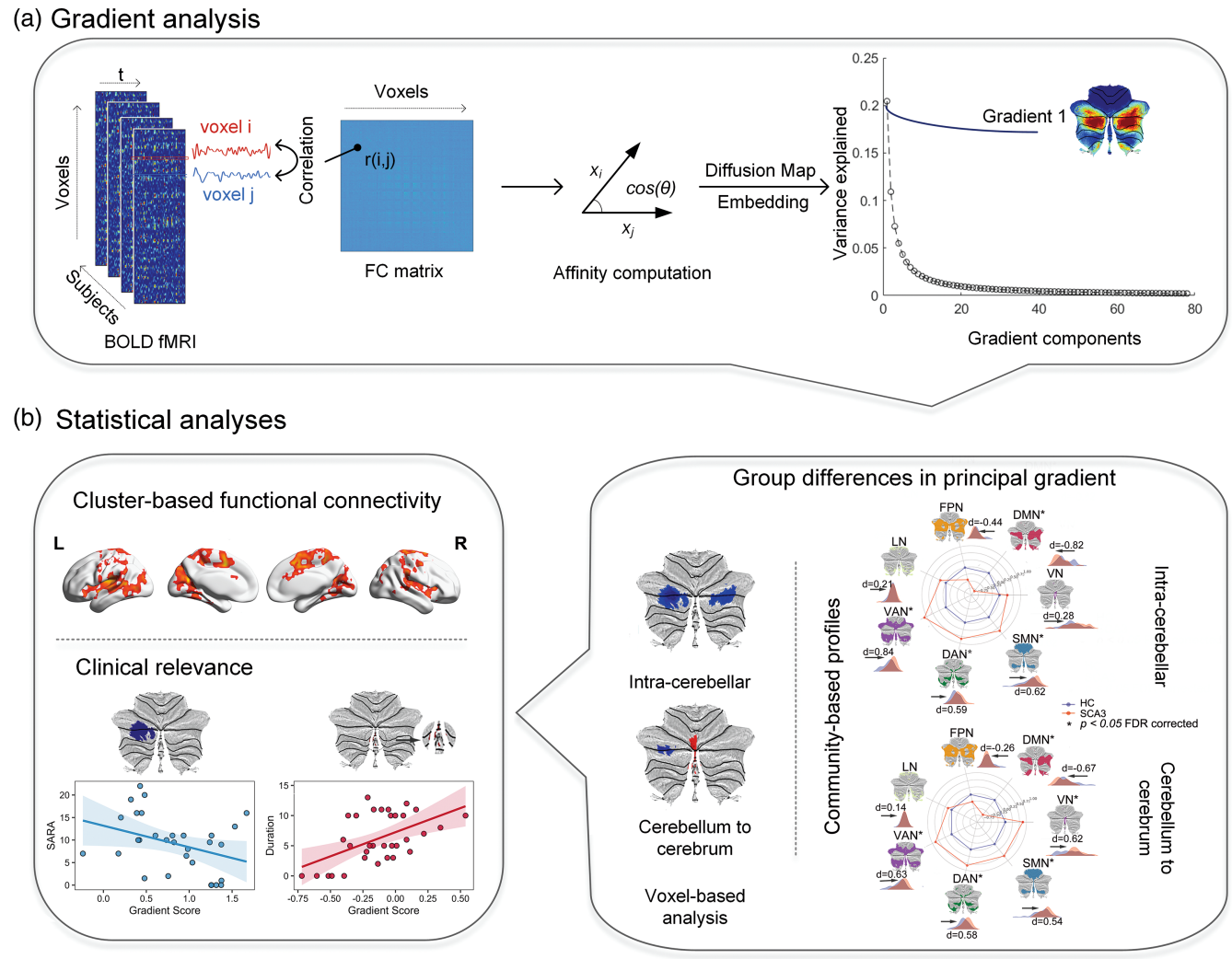

FIGURE 1 Overview of gradients analysis pipeline. (a) Functional connectivity (FC) matrices were derived for each participant from resting-state functional MRI data. Then cosine similarity was used to build the affinity matrix, and diffusion embedding map was used to capture the explained variance that was sorted. Finally, the principal functional gradient was projected back to the cerebellar flatmap. (b) Statistical analyses to test hypotheses.

TABLE 1 Demographic and clinical characteristics.

Demographics	SCA3 ($n = 35$)	HC ($n = 48$)	Comparison
	Mean ± SD	Mean ± SD	SCA3 vs. HC
Gender (male/female)	17/18	24/24	$\chi^2 = 0.13$ ($p = .90$)
Age	40.37 ± 12.98	40.29 ± 11.60	$t = 0.03$ ($p = .47$)
Duration (years)	6.71 ± 4.66		
CAG repeat	79.97 ± 6.59		
FD	0.15 ± 0.07	0.13 ± 0.08	$U = 598$ ($p = .03$)
SARA	10.44 ± 8.43		

Note: Values are mean ± standard deviation. The χ^2 value for gender distribution was obtained by the chi-square test. The *U* values were obtained by the Mann–Whitney *U* test.
Abbreviations: FD, framewise displacements; HC, healthy controls; SARA, scale for the assessment and rating of ataxia; SCA3, patients with spinocerebellar ataxia type 3.

3 | RESULTS

3.1 | Gray matter volume loss of SCA3 and HC

Between-group differences of whole-brain GMV and cGMV of SCA3 and HC groups were shown in Figure S1. The SCA3 group exhibited significantly reduced whole-brain GMV ($p < .001$) and decreased cGMV ($p < .001$) compared to the HC group.

3.2 | The principal gradient in patients with SCA3 and HC

The diffusion map embedding method was applied to intra-cerebellar and cerebellar-cerebral connectomes derived from resting-state fMRI in each subject to obtain a set of gradients. We focused on the principal gradient explaining the majority of the connectome variance in the intra-cerebellar gradients (20.17% ± 6.65%) and cerebellar-cerebral connectome (20.97% ± 6.08%) gradients. There was no significant difference in the explained variance of intra-cerebellar and cerebellar-cerebral principal gradients between SCA3 and HC groups (Mann–Whitney *U* test: intra-cerebellar gradient: $p = .31$; cerebellar-cerebral gradient: $p = .20$; Figure S2). After aligning the individual gradients to a group template from all participants, the principal gradient was mapped back onto the cerebellar cortex in both SCA3 and HC groups. FC gradients within the cerebellum and cerebellar-cerebral had similar spatial distributions. Both SCA3 patients and HCs showed a progressive axis of connectivity change extending along lobules I–IV (unimodal regions) in the cerebellar anterior lobe towards Crus I/II and lobule IX (transmodal regions) in the cerebellar posterior lobe (Figure 2a,d), which was in agreement with previous studies (Dong et al., 2020; Guell et al., 2018).

3.3 | Altered principal gradient in patients with SCA3

Global histogram analyses were performed to compare the gradient distribution between the SCA3 and HC groups. In patients with SCA3, we observed a compressed pattern of the principal gradient in both intra-cerebellar and cerebellar-cerebral gradients compared to HCs (Figure 2b,e). This compression was manifested as a shrinkage at both ends of the principal gradient axis and an increase in the value of the middle axis.

To explore the perturbation of cerebellar gradients in SCA3, we compared the principal gradient between groups at both voxel and network levels. At the large-scale network level, we statistically compared the principal gradients of each network using the canonical cerebellar functional network community decomposition (Buckner et al., 2011). In the network-based analysis of intra-cerebellar principal gradients, we found significant reductions of principal gradient scores in the default mode network (Cohen's $d = -0.82$, $p = .01$, FDR corrected) and increases in the ventral attention network (Cohen's $d = 0.84$, $p = .02$, FDR corrected) and dorsal attention network (Cohen's $d = 0.59$, $p = .01$, FDR corrected), as well as significant increases in somatomotor network (Cohen's $d = 0.62$, $p = .01$, FDR corrected) in patients with SCA3 compared with HCs (Figure 2c). Similar findings were found in the cerebellar-cerebral gradients of SCA3 (Figure 2f), with apparent decreases of gradient scores in the default mode network (Cohen's $d = -0.67$, $p = .01$, FDR corrected) and increases in the ventral attention network (Cohen's $d = 0.63$, $p = .02$, FDR corrected), dorsal attention network (Cohen's $d = 0.58$, $p = .01$, FDR corrected), visual network (Cohen's $d = 0.62$, $p = .02$, FDR corrected) and somatomotor network (Cohen's $d = 0.54$, $p = .01$, FDR corrected). The network-level results of both intra-cerebellar and cerebellar-cerebral gradients aligned with the overall global histogram distribution, indicating an abnormal compression of the principal gradients. Consistent findings were obtained when the network-based analysis of principal gradients repeated without controlling for cGMV (Figure S3).

Patients with SCA3 showed a similar mixed pattern of principal gradient increase and decrease in both intra-cerebellar and cerebellar-cerebral voxel-level comparisons. Specifically, abnormal reduction in principal gradient scores in SCA3 was observed mainly in the bilateral Crus I/II of transmodal areas. Conversely, significantly increased gradient scores in SCA3 were detected in the right lobule VIII and vermis involved in early integration (Figure 3a,d). Importantly, when controlling for cGMV (Figure 3b,e), all results remained significant, with the exceptions of increased intra-cerebellar gradient scores in vermis and right lobules VIII, and increased cerebellar-cerebral gradient scores in right lobules VIII in SCA3 patients (which were not significant after correcting for cGMV). Figure 3c,f displayed scatterplots that depicted the between-group differences before and after controlling for cGMV, with the x-axis representing the principal gradient of HC and the y-axis representing the principal gradient of SCA3. Table 2 listed the aberrant brain regions (10,000 permutations, $p < .05$, TFCE corrected) showing significant between-group differences in principal gradient scores, indicating regions with either elevated or reduced gradient scores in the SCA3 group.

3.4 | Relation to clinical symptoms

Figure 4a,b illustrate the regions showing group differences in gradient scores that correlated with SARA scales and duration of disease in the SCA3 group (see Table S1 for details). Higher scores in SARA indicated increased severity of symptoms and worse clinical behavior. The principal intra-cerebellar gradient score of the left Crus II/I negatively correlated with SARA ($r = -.48$, $p = .04$, FDR corrected) scale. Similarly, the principal intra-cerebellar gradient score of the right Crus II/I also showed a negative correlation with SARA ($r = -.50$, $p = .04$, FDR corrected) scale. A positive correlation was found between the principal cerebellar-cerebral gradient scores of lobule VIII and the disease duration ($r = .48$, $p = .04$, FDR corrected). Additionally, no associations were observed between FD and altered gradient scores (all p values were greater than .20, Figure S4), demonstrating that

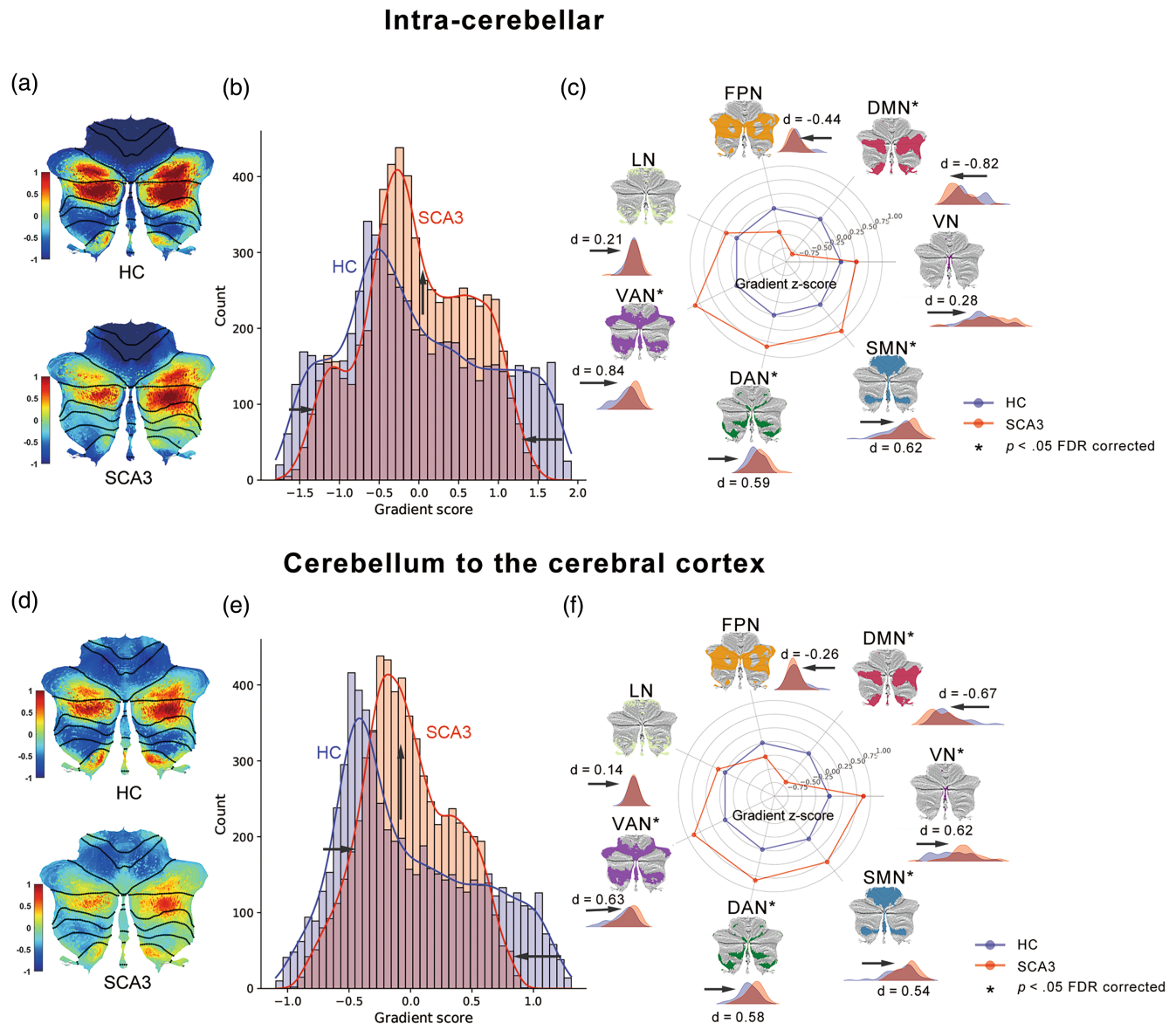

FIGURE 2 Cerebellar connectome gradients and network distribution in HCs and SCA3. (a, d) Cerebellar connectome gradients mapping in SCA3 and HCs based on intra-cerebellar functional connectome (a) and cerebellar-cerebral functional connectome (d). Color similarity denotes connectivity similarity. B and E: Global histograms of intra-cerebellar (b) and cerebellar-cerebral (e) gradients in SCA3 patients and HCs. SCA3 patients exhibited a compressed principal gradient, as reflected by the suppressed extreme values and the increased values in the mid-range in SCA3 compared with HCs. C and F: Network-based z-score analysis of intra-cerebellar (c) and cerebellar-cerebral (f) gradient scores (relative to healthy controls) depicted by radar plots both illustrated significant reductions in default mode network ($p < 0.05$, FDR corrected) and an increase in the ventral attention network, dorsal attention network, and sensorimotor network ($p < .05$, FDR corrected) in SCA3. And Cohen's *d* was computed.

gradient differences between SCA3 and HC groups were not influenced by head motion.

3.5 | Connectivity differences based on gradient findings

The result of functional connectivity analysis that focused on clusters of significant gradient alterations revealed hyper-connectivity changes. Specifically, the two clusters located in the left cerebellar Crus I/II and right cerebellar Crus I/II, which showed decreased principal gradients in SCA3, presented hyper-connectivity changes with both unimodal and transmodal areas in the cerebellum and cerebrum. These areas include cerebellar bilateral lobules VIII/VII/VI/IX, vermis, bilateral supplementary motor areas, precuneus, left middle temporal gyrus, right posterior cingulate, and so on. (Figure 4c; 10,000 permutations, $p < .05$, TFCE corrected).

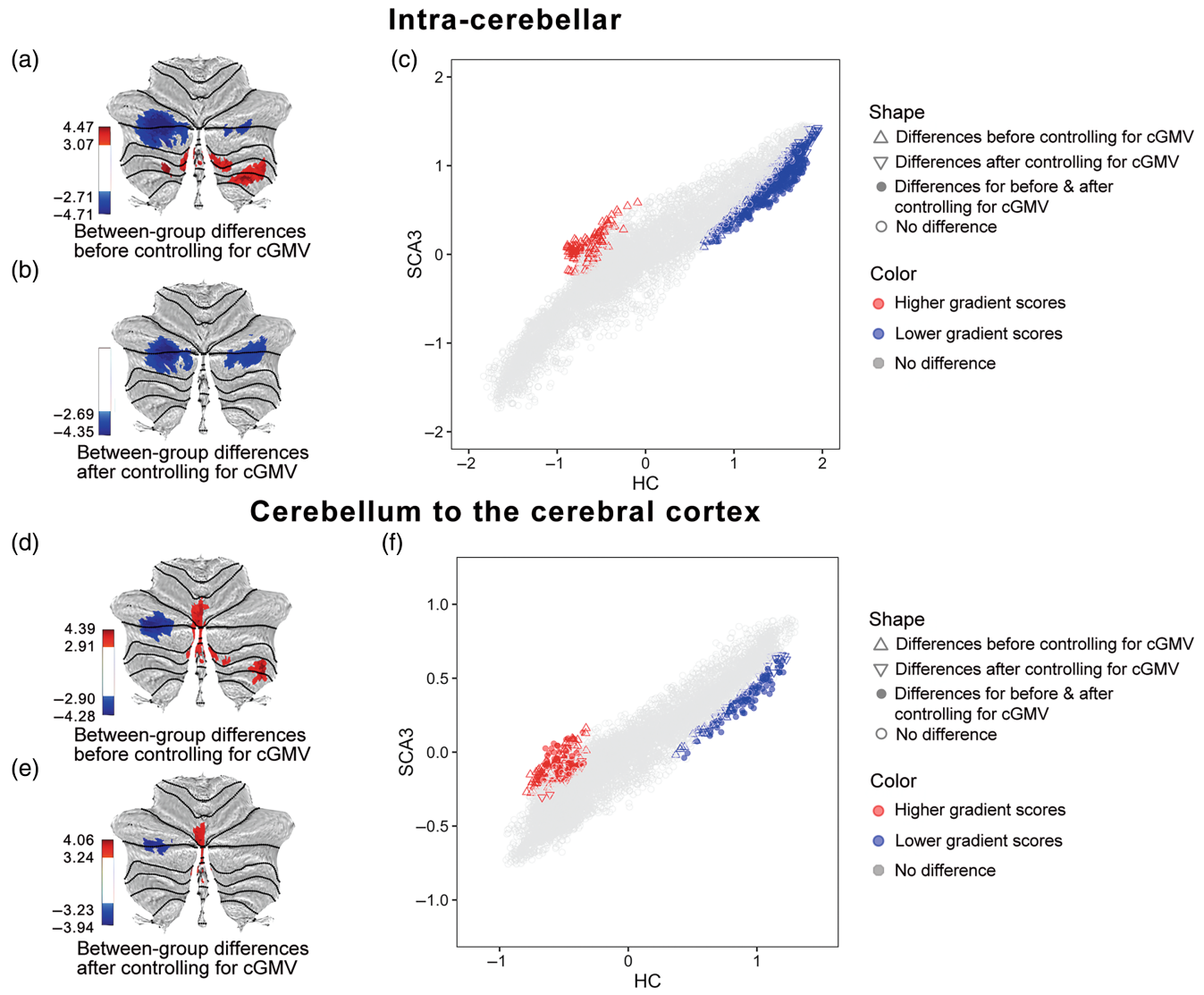

FIGURE 3 Cerebellar gray matter atrophy effect on case–control gradient differences. (a, d) Case–control differences of intra-cerebellar gradients and cerebellar-cerebral gradients without controlling for cGMV. (b, e) Case–control differences of intra-cerebellar gradients and cerebellar-cerebral gradients after controlling for cGMV. (c, f) Scatterplot depicted the differences for principle gradient scores before and after correction for cGMV (x-axis: cerebellar gradient of HCs; y-axis: cerebellar gradient of SCA3). Scatterplot colors corresponded to the group differences map, as shown in the figure: higher gradient scores in SCA3 (red) and lower gradient scores in SCA3 (blue) compared to HCs. Scatter shapes corresponded to four situations that existed before and after controlling the GMV, as described in the label in the scatterplot. cGMV, cerebellar gray matter volume.

4 | DISCUSSION

This is the first study that explored the functional connectome hierarchy of the cerebellum with SCA3 populations. We used gradient analysis to investigate the hierarchical organization of cerebellar function in SCA3 and examined its perturbations, from which we drew three main findings, as follows: (1) Compared to HCs, SCA3 patients exhibited abnormal compression of the gradient axis of macroscale organization in the cerebellum at both the network and voxel levels, suggesting imbalances in the hierarchical patterns of cerebellar functional organization between the unimodal and transmodal systems. (2) The compression of principal gradients in SCA3 patients appeared to arise from a combination of structural atrophy and intrinsic neuronal changes. (3) In both the intra-cerebellar and cerebellar-cerebral gradients, altered gradients of aberrant regions were correlated with the severity of ataxia symptoms and the disease duration.

In contrast to using functional connectivity to reflect temporal correlation between the activities in different brain regions, functional gradients provide an integrated view to further analyze the continuous transitions between functional connectivity patterns in a low-dimensional space (Guell et al., 2018; Huntenburg et al., 2018; Margulies et al., 2016). Multimodal studies have strongly suggested that gradients can reveal the functional hierarchy underlying information processing (Guell et al., 2018; Huntenburg et al., 2018; Margulies

TABLE 2 Abnormal principal gradient regions in SCA3 patients.

Cluster	Brain regions	*T* value	Voxels	Peak MNI coordinates		
				X	Y	Z
Results before controlling for cGMV						
Intra-cerebellar principal functional gradient						
Patients > Controls						
1	Right lobules VIII, Vermis	4.47	44	−3	−75	−39
2	Right lobules VIII	4.33	75	18	−54	−54
Patients < Controls						
3	Left Crus II, Crus I	−4.71	360	−36	−78	−30
4	Right Crus I	−3.49	18	33	−69	−33
Cerebellar-cerebral principal functional gradient						
Patients > Controls						
1	Right lobules VI/VIII, Vermis	4.39	65	0	−72	−45
2	Right lobule VIII	4.21	31	36	−48	−54
Patients < Controls						
3	Left Crus II, Crus I	−4.28	105	−39	−84	−30
Results after controlling for cGMV						
Intra-cerebellar principal functional gradient						
Patients < Controls						
1	Left Crus II, Crus I	−4.35	264	−30	−78	−33
2	Right Crus II, Crus I	−3.37	162	39	−75	−39
Cerebellar-cerebral principal functional gradient						
Patients > Controls						
1	Left lobules VI, Vermis	3.95	18	−3	−69	−24
2	Left lobules VIII, Vermis	4.06	11	−3	−75	−36
Patients < Controls						
3	Left Crus I/II	−3.75	18	−42	−69	−36

et al., 2016; Paquola et al., 2019; Vogel et al., 2020; Vos de Wael et al., 2018; Wang, 2020), thus ultimately advancing our understanding of functional abnormalities under neurological and neuropsychiatric conditions (Bayrak et al., 2019; Bernhardt et al., 2022; Dong et al., 2020; Hong et al., 2019; Meng et al., 2021). In this study, we employed the functional gradient to demonstrate the compression of cerebellar functional hierarchical organization in SCA3. The compressed pattern of cerebellar functional organization indicated a less differentiated global hierarchy in the cerebellum of SCA3, showing a stronger global shift from unimodal to transmodal areas. Our results not only supported previous findings using predefined networks in SCA3 but also added the topographical description of cerebellar macroscale hierarchy in SCA3, thereby providing a new perspective to understand the functional abnormalities in this condition (Chen et al., 2022; Margulies et al., 2016; Mesulam, 1998).

A rather consistent finding from intra-cerebellar and cerebellar-cerebral principal gradient analyses was that SCA3 patients exhibited a compressed gradient pattern at the network level along the cerebellar functional hierarchical organization axis. Evident compression was seen in the middle and right edges of the principal gradient axis, corresponding to the task-active or default mode network (DMN) of the cerebellum. Significant increases in intra-cerebellar and cerebellar-cerebral gradient scores were also found in somatomotor network in SCA3 patients. The reduced principal gradients in DMN may be due to the fact that SCA3 pathological alterations utilize non-motor resources to mitigate motor impairments (Chen et al., 2022). A recent fMRI research using a paradigm of bilateral audio-paced thumb movements revealed decreased movement synchronization in SCA3 patients, supporting the functional rearrangement of the motor network (Duarte et al., 2016). Likewise, the network shift in activation from the vermis to the lateral cerebellum in moderate-to-severe has been reported in SCA6 (Falcon et al., 2016). Therefore, the compressed cerebellar hierarchy possibly reflects a compensatory mechanism. The ventral attention network and dorsal attention network of the cerebellum are relevant for stimulus-driven and goal-oriented attention in attentional and executive processing, respectively (Guell & Schmahmann, 2020). It has been demonstrated that the activity in DMN is reversely correlated to that of attentional and executive processing during attentional demanding tasks

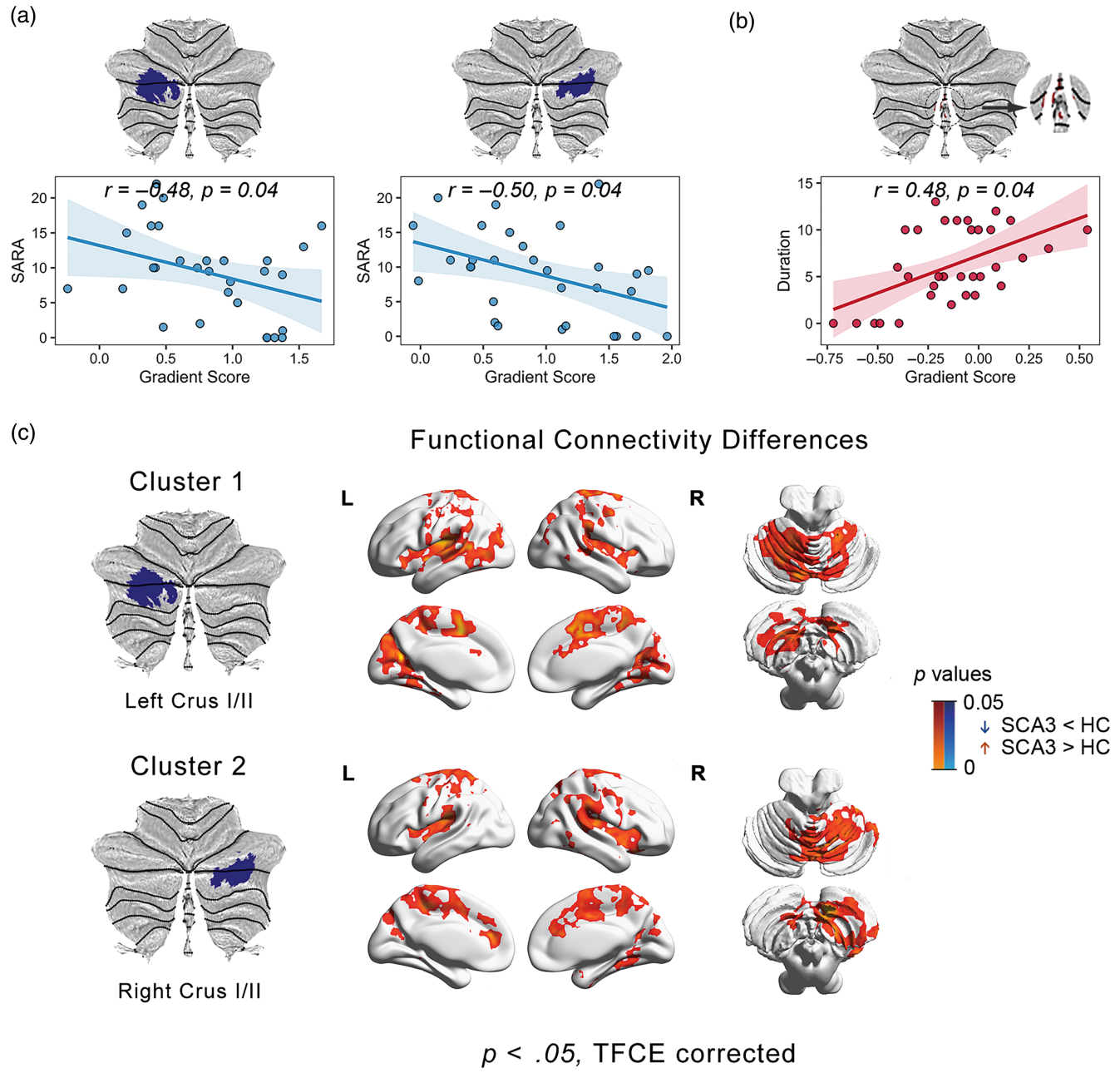

FIGURE 4 Clinical relevance and post-hoc functional connectivity analysis of cerebellar gradients in SCA3. (a, b) Correlations between gradient scores and clinical variables. (a) Negative correlation between intra-cerebellar gradient scores in left Crus I/II and SARA scores (left), and a negative correlation between intra-cerebellar gradient scores in right Crus I/II and SARA scores (right). (b) Positive correlation between cerebellar-cerebral gradient scores in vermis and disease duration. (c) Group differences between patients with SCA3 and HCs in functional connectivity based on the voxel level gradients comparing resulting clusters. The warm and cold colors of clusters represent increased and decreased regions, respectively.

(Gusnard & Raichle, 2001). Our results of increased gradients in the task active network and reduced gradients in the DMN of the cerebellum may suggest an irregular functional switch between these functional systems in SCA3. Similar irregularities were observed in Essential tremor (Passamonti et al., 2011) and Alzheimer patients (Samson & Claassen, 2017). Another interpretation is that these networks with increased gradients in SCA3 were over-engaged to compensate for the impaired behavioral deficits (Chen et al., 2022).

We also analyzed the abnormal patterns of intra-cerebellar gradients and cerebellar-cerebral gradients in SCA3 patients at the voxel level. In general, abnormally reduced intra-cerebellar and cerebellar-cerebral gradient scores were observed mainly in the Crus I and Crus II, overlapping with DMN in patients with SCA3 compared to HCs. SCA3 participants also showed stronger FC between the cerebellar default network and the remaining brain networks, indicating the differentiated global hierarchy between the cerebellar default network

and other functional brain networks. However, SCA3 patients demonstrated a mixed pattern of the principal cerebellar-cerebral gradient increase and decrease, presenting increased principal gradient scores in unimodal areas (left lobules VI/VIII and vermis) and reduced gradient scores in transmodal areas (posterior left Crus I/II) of the cerebellum. Most of these locations match previous SCA3 morphometry, task activation, and resting-state analyses (Guo et al., 2020; Piccinin et al., 2020; Rezende et al., 2018; Stefanescu et al., 2015; Wan et al., 2020; Yap et al., 2022).

Of note, the altered gradient patterns, characterized by decreased intra-cerebellar gradient scores in the bilateral Crus I/II, decreased cerebellar-cerebral gradient scores in the left CrusI/II, and increased cerebellar-cerebral gradient scores in the vermis, remained consistent, whereas increased intra-cerebellar and cerebellar-cerebral gradient scores in right lobule VIII were no longer significant after controlling for cGMV. Our findings highlighted the impact of reduced cGMV on the aberrant cerebellar functional organization in SCA3 patients. Brain anatomy could constrain the flow of functional connectivity or functional activation (Gu et al., 2021; Pang et al., 2023). Previous studies on SCAs have reported associations between volume loss and abnormalities in cerebellar-related functional connectivity (Cocozza et al., 2015; Guo et al., 2023; Hernandez-Castillo et al., 2014). Additionally, some studies have proposed that abnormal patterns in functional connectomes may precede structural degeneration (Worbe, 2015; Zhou et al., 2012). Our results suggested a complex imbalance in cerebellar hierarchical organization in SCA3 patients, with changes in both structural atrophy and intrinsic neurons contributing. This finding provided another mechanism to explain the observed cerebellar functional hierarchical anomalies in SCA3 patients. It is important to note that there is no direct causal relationship between volume loss and functional hierarchical anomalies. Further longitudinal studies are needed to provide causal evidence.

Correlation analyses with SARA scores suggested that the compressed cerebellar functional hierarchy may underlie the motor deficits observed in SCA3. In particular, higher clinical severity was associated with a more compressed pattern of intra-cerebellar functional gradients, as shown by the decreased gradient scores in bilateral Crus I/II in SCA3. The cerebellum plays a vital role in motor coordination, which smooths out our movements and makes them more accurate. The process of movement coordination of the cerebellum follows a hierarchical organization: (1) acquire information about the motor plan from the cerebrum; (2) get sense information from the proprio receptors and compare it with the motor plan; and (3) send feedback to motor areas of the cerebrum to make the movement match the motor plan (Friston et al., 2017; Hutchinson & Barrett, 2019). These cerebellar regions with abnormal gradients in our findings are involved in motor coordination; they serve high-order motor control. The Crus I/II is located in the posterior cerebellum, and its coordination is critical in accomplishing many high-order functions (D'Mello et al., 2020). In particular, we found increased FC strength between bilateral Crus I/II and motor-related areas, including the precuneus and supplementary motor areas, denoting the abnormalities of motor coordination. We also found a positive relationship between elevated scores of cerebellar-cerebral gradient in vermis and the disease duration, thereby associating cerebellar functional hierarchical irregularities with disease burden. More precisely, the Purkinje cells are involved in comparing the sense information with the motor plan (Kandel et al., 2021), whereas the Purkinje cells in vermis were most affected by SCA6 (Panouilleres et al., 2018) and also appeared to be more sensitive to neurodegenerative changes of SCA3 (Guo et al., 2020).

The compressed functional hierarchy found in SCA3 might impair the information processing between intra-cerebellar and cerebellar-cerebral functional systems and further influence the calculation for coordinating actions, namely as feedforward processing. Impaired feedforward processing may result in an increased demand for actual movement correction, which is a hallmark of ataxia. Thus, our results could imply that deficits in feedforward processing may impair the integration of information, with cascading effects on feedback processing in high-order functions, ultimately leading to the deficits observed in SCA3, as suggested in a metabolic topography study of SCA3 (Meles et al., 2018). Furthermore, a recent 7 T fMRI study demonstrated the somatotopic organization of the five body parts (toes, little fingers, thumbs, tongue, and eyes) in the cerebellum (Boillat et al., 2020). Abnormalities of the functional gradient in these regions might in part account for the ataxia phenotypes, such as poor coordination of hands, speech, walking, and eye movements. These findings suggested that the alterations in the functional hierarchy of the cerebellum may underlie ataxic symptoms in SCA3.

The current study has several limitations. Firstly, we did not assess the trajectory of changes in gradients throughout the progression of the disease. Previous studies have indicated that structural brain damage in SCA3 exists at different stages of the disease (Guo et al., 2020; Rezende et al., 2018). Functional gradient compression abnormalities may progress from preclinical to early and late stages of the disease. Future longitudinal studies could investigate how cerebellar gradient patterns in SCA3 change over time. Secondly, only gray matter volume was added as a covariate in the control analysis to explore the effect of volume loss. Prior research has substantiated a close relationship between the widespread destruction of white matter structural integrity and the clinical severity of ataxia symptoms in SCA3 (Kang et al., 2014). Future studies should examine how structural changes within the white matter in SCA3 impact the current findings. Furthermore, although we demonstrated the impact of volume loss by adding whole-brain GMV and cGMV as covariates in between-group gradient comparison in SCA3, employing voxel-wise analysis of volume loss can capture gray matter atrophy with high regional specificity and is more suitable for a comprehensive examination of the interactions between functional and structural changes. Future studies should compare the results both before and after voxel-wise corrections for volume loss to validate our findings. Finally, although we found some relevant evidence supporting a link between gradient scores and ataxia symptoms, the correlation of our study does not allow us to establish a causal relationship between the principal gradient and the pathogenesis of SCA3. To explore the causal relationship between alterations in cerebellar gradients and the pathophysiology of SCA3, future neurostimulation studies could be conducted.

5 | CONCLUSION

This study leveraging the connectome gradient suggested the presence of compressed cerebellar hierarchical organization in SCA3 across different scales. The compressed pattern of principal gradients showed reasonable association with clinical ataxia symptoms, which might reflect the feedforward processing deficits in high-order motor control in SCA3. Our results may help contribute to our growing understanding of SCA3 pathophysiology and provide a novel insight into the functional abnormalities of the cerebellum in SCA3.

AUTHOR CONTRIBUTIONS

Xinyuan Liu: Research project (conception, execution), statistical analysis (design, execution), manuscript preparation (writing of the first draft). **Jing Guo:** Research project (conception, execution), statistical analysis (review and critique), manuscript preparation (review and critique). **Zhouyu Jiang:** Statistical analysis (review and critique). **Xingli Liu:** Manuscript preparation (review and critique). **Hui Chen:** Research project (execution). **Yuhan Zhang:** Research project (execution). **Qing Gao:** Statistical analysis (review and critique), manuscript preparation (review and critique). **Jian Wang:** Research project (conception, organization, execution), manuscript preparation (review and critique). **Chen Liu:** Research project (conception, organization, execution), statistical analysis (review and critique), manuscript preparation (review and critique). **Huafu Chen:** Research project (conception, organization, execution), statistical analysis (review and critique), manuscript preparation (review and critique).

ACKNOWLEDGMENTS

This work was supported by the National Science and Technology Major Project (2021ZD0201701), the Natural Science Foundation of China (62333003, 62036003, 82121003, 62173070, 82071910, 81601478), Senior Medical Talents Program of Chongqing for Young and Middle-aged (414Z395) and Young and Middle-aged Senior Medical Talents studio of Chongqing, and the Medical-Engineering Cooperation Funds from University of Electronic Science and Technology of China (ZYGX2021YGLH201), Innovation Team and Talents Cultivation Program of National Administration of Traditional Chinese Medicine (ZYYCXTD-D-202003).

CONFLICT OF INTEREST STATEMENT

The authors declare no disclosures relevant to the manuscript.

DATA AVAILABILITY STATEMENT

Yes, all the data could be available only for research purposes.

ORCID

Chen Liu https://orcid.org/0000-0001-5149-2496
Qing Gao https://orcid.org/0000-0001-8504-6128
Huafu Chen https://orcid.org/0000-0002-4062-4753

REFERENCES

Ashburner, J., & Friston, K. J. (2005). Unified segmentation. *NeuroImage*, *26*, 839–851.

Ashburner, J., & Friston, K. J. (2011). Diffeomorphic registration using geodesic shooting and Gauss-Newton optimisation. *NeuroImage*, *55*, 954–967.

Bayrak, S., Khalil, A. A., Villringer, K., Fiebach, J. B., Villringer, A., Margulies, D. S., & Ovadia-Caro, S. (2019). The impact of ischemic stroke on connectivity gradients. *NeuroImage Clinical*, *24*, 101947.

Bernhardt, B. C., Smallwood, J., Keilholz, S., & Margulies, D. S. (2022). Gradients in brain organization. *NeuroImage*, *251*, 118987.

Boillat, Y., Bazin, P. L., & van der Zwaag, W. (2020). Whole-body somatotopic maps in the cerebellum revealed with 7T fMRI. *NeuroImage*, *211*, 11.

Buckner, R. L., Krienen, F. M., Castellanos, A., Diaz, J. C., & Yeo, B. T. (2011). The organization of the human cerebellum estimated by intrinsic functional connectivity. *Journal of Neurophysiology*, *106*, 2322–2345.

Chen, H., Dai, L., Zhang, Y., Feng, L., Jiang, Z., Wang, X., Xie, D., Guo, J., Chen, H., Wang, J., & Liu, C. (2022). Network reconfiguration among cerebellar visual, and motor regions affects movement function in spinocerebellar ataxia type 3. *Frontiers in Aging Neuroscience*, *14*, 773119.

Chen, X., Lu, B., & Yan, C. G. (2018). Reproducibility of R-fMRI metrics on the impact of different strategies for multiple comparison correction and sample sizes. *Human Brain Mapping*, *39*, 300–318.

Cocozza, S., Sacca, F., Cervo, A., Marsili, A., Russo, C. V., Giorgio, S. M., De Michele, G., Filla, A., Brunetti, A., & Quarantelli, M. (2015). Modifications of resting state networks in spinocerebellar ataxia type 2. *Movement Disorders*, *30*, 1382–1390.

Coifman, R. R., Lafon, S., Lee, A. B., Maggioni, M., Nadler, B., Warner, F., & Zucker, S. W. (2005). Geometric diffusions as a tool for harmonic analysis and structure definition of data: Diffusion maps. *Proceedings of the National Academy of Sciences of the United States of America*, *102*, 7426–7431.

Diedrichsen, J. (2006). A spatially unbiased atlas template of the human cerebellum. *NeuroImage*, *33*, 127–138.

D'Mello, A. M., Gabrieli, J. D. E., & Nee, D. E. (2020). Evidence for hierarchical cognitive control in the human cerebellum. *Current Biology*, *30*, 1881–1892.e3.

Dong, D., Luo, C., Guell, X., Wang, Y., He, H., Duan, M., Eickhoff, S. B., & Yao, D. (2020). Compression of cerebellar functional gradients in schizophrenia. *Schizophrenia Bulletin*, *46*, 1282–1295.

Duarte, J. V., Faustino, R., Lobo, M., Cunha, G., Nunes, C., Ferreira, C., Januario, C., & Castelo-Branco, M. (2016). Parametric fMRI of paced motor responses uncovers novel whole-brain imaging biomarkers in spinocerebellar ataxia type 3. *Human Brain Mapping*, *37*, 3656–3668.

Falcon, M. I., Gomez, C. M., Chen, E. E., Shereen, A., & Solodkin, A. (2016). Early cerebellar network shifting in spinocerebellar ataxia type 6. *Cerebral Cortex*, *26*, 3205–3218.

Friston, K., FitzGerald, T., Rigoli, F., Schwartenbeck, P., & Pezzulo, G. (2017). Active inference: A process theory. *Neural Computation*, *29*, 1–49.

Gaser, C., Dahnke, R., Thompson, P. M., Kurth, F., Luders, E., & Alzheimer's Disease Neuroimaging Initiative. (2022). CAT—A computational anatomy toolbox for the analysis of structural MRI data. *bioRxiv*. https://doi.org/10.1101/2022.06.11.495736

Gu, Z. J., Jamison, K. W., Sabuncu, M. R., & Kuceyeski, A. (2021). Heritability and interindividual variability of regional structure-function coupling. *Nature Communications*, *12*, 12.

Guell, X., & Schmahmann, J. (2020). Cerebellar functional anatomy: A didactic summary based on human fMRI evidence. *Cerebellum*, *19*, 1–5.

Guell, X., Schmahmann, J. D., Gabrieli, J., & Ghosh, S. S. (2018). Functional gradients of the cerebellum. *eLife*, *7*, e36652.

Guo, J., Chen, H., Biswal, B. B., Guo, X., Zhang, H., Dai, L., Zhang, Y., Li, L., Fan, Y., Han, S., Liu, J., Feng, L., Wang, Q., Wang, J., Liu, C., & Chen, H. (2020). Gray matter atrophy patterns within the cerebellum-neostriatum-cortical network in SCA3. *Neurology*, *95*, e3036–e3044.

Guo, J., Jiang, Z. Y., Liu, X. Y., Li, H. R., Biswal, B. B., Zhou, B., Sheng, W., Gao, Q., Chen, H., Fan, Y. S., Zhu, W., Wang, J., Chen, H., & Liu, C. (2023). Cerebello-cerebral resting-state functional connectivity in spinocerebellar ataxia type 3. *Human Brain Mapping*, *44*, 927–936.

Gusnard, D. A., & Raichle, M. E. (2001). Searching for a baseline: Functional imaging and the resting human brain. *Nature Reviews. Neuroscience*, *2*, 685–694.

Hahamy, A., Calhoun, V., Pearlson, G., Harel, M., Stern, N., Attar, F., Malach, R., & Salomon, R. (2014). Save the global: Global signal connectivity as a tool for studying clinical populations with functional magnetic resonance imaging. *Brain Connectivity*, *4*, 395–403.

Hernandez-Castillo, C. R., Alcauter, S., Galvez, V., Barrios, F. A., Yescas, P., Ochoa, A., Garcia, L., Diaz, R., Gao, W., & Fernandez-Ruiz, J. (2013). Disruption of visual and motor connectivity in spinocerebellar ataxia type 7. *Movement Disorders*, *28*, 1708–1716.

Hernandez-Castillo, C. R., Galvez, V., Morgado-Valle, C., & Fernandez-Ruiz, J. (2014). Whole-brain connectivity analysis and classification of spinocerebellar ataxia type 7 by functional MRI. *Cerebellum & Ataxias*, *1*, 2.

Hong, S. J., Vos de Wael, R., Bethlehem, R. A. I., Lariviere, S., Paquola, C., Valk, S. L., Milham, M. P., Di Martino, A., Margulies, D. S., Smallwood, J., & Bernhardt, B. C. (2019). Atypical functional connectome hierarchy in autism. *Nature Communications*, *10*, 1022.

Huntenburg, J. M., Bazin, P. L., & Margulies, D. S. (2018). Large-scale gradients in human cortical organization. *Trends in Cognitive Sciences*, *22*, 21–31.

Hutchinson, J. B., & Barrett, L. F. (2019). The power of predictions: An emerging paradigm for psychological research. *Current Directions in Psychological Science*, *28*, 280–291.

Jenkinson, M., Bannister, P., Brady, M., & Smith, S. (2002). Improved optimization for the robust and accurate linear registration and motion correction of brain images. *NeuroImage*, *17*, 825–841.

Kandel, E. R., Koester, J. D., Mack, S. H., & Siegelbaum, S. A. (2021). *The cerebellum. In principles of neural science, 6e*. McGraw Hill.

Kang, J. S., Klein, J. C., Baudrexel, S., Deichmann, R., Nolte, D., & Hilker, R. (2014). White matter damage is related to ataxia severity in SCA3. *Journal of Neurology*, *261*, 291–299.

Klockgether, T., Mariotti, C., & Paulson, H. L. (2019). Spinocerebellar ataxia. *Nature Reviews Disease Primers*, *5*, 24.

Langs, G., Golland, P., & Ghosh, S. S. (2015). Predicting activation across individuals with resting-state functional connectivity based multi-atlas label fusion. *Medical Image Computing and Computer-Assisted Intervention*, *9350*, 313–320.

Margulies, D. S., Ghosh, S. S., Goulas, A., Falkiewicz, M., Huntenburg, J. M., Langs, G., Bezgin, G., Eickhoff, S. B., Castellanos, F. X., Petrides, M., Jefferies, E., & Smallwood, J. (2016). Situating the default-mode network along a principal gradient of macroscale cortical organization. *Proceedings of the National Academy of Sciences of the United States of America*, *113*, 12574–12579.

Meles, S. K., Kok, J. G., De Jong, B. M., Renken, R. J., de Vries, J. J., Spikman, J. M., Ziengs, A. L., Willemsen, A. T. M., van der Horn, H. J., Leenders, K. L., & Kremer, H. P. (2018). The cerebral metabolic topography of spinocerebellar ataxia type 3. *Neuroimage Clinical*, *19*, 90–97.

Meng, Y., Yang, S., Chen, H., Li, J., Xu, Q., Zhang, Q., Lu, G., Zhang, Z., & Liao, W. (2021). Systematically disrupted functional gradient of the cortical connectome in generalized epilepsy: Initial discovery and independent sample replication. *NeuroImage*, *230*, 117831.

Mesulam, M. M. (1998). From sensation to cognition. *Brain*, *121*, 1013–1052.

O'Callaghan, C., Hornberger, M., Balsters, J. H., Halliday, G. M., Lewis, S. J., & Shine, J. M. (2016). Cerebellar atrophy in Parkinson's disease and its implication for network connectivity. *Brain*, *139*, 845–855.

Olivito, G., Cercignani, M., Lupo, M., Iacobacci, C., Clausi, S., Romano, S., Masciullo, M., Molinari, M., Bozzali, M., & Leggio, M. (2017). Neural substrates of motor and cognitive dysfunctions in SCA2 patients: A network based statistics analysis. *Neuroimage Clinical*, *14*, 719–725.

Pang, J. C., Aquino, K. M., Oldehinkel, M., Robinson, P. A., Fulcher, B. D., Breakspear, M., & Fornito, A. (2023). Geometric constraints on human brain function. *Nature*, *30*, 566–574.

Panouilleres, M. T. N., Joundi, R. A., Benitez-Rivero, S., Cheeran, B., Butler, C. R., Nemeth, A. H., Miall, R. C., & Jenkinson, N. (2018). Sensorimotor adaptation as a behavioural biomarker of early spinocerebellar ataxia type 6 (vol 7, 2017). *Scientific Reports*, *8*, 1.

Paquola, C., Vos De Wael, R., Wagstyl, K., Bethlehem, R. A. I., Hong, S. J., Seidlitz, J., Bullmore, E. T., Evans, A. C., Misic, B., Margulies, D. S., & Smallwood, J. (2019). Microstructural and functional gradients are increasingly dissociated in transmodal cortices. *PLoS Biology*, *17*, e3000284.

Passamonti, L., Novellino, F., Cerasa, A., Chiriaco, C., Rocca, F., Matina, M. S., Fera, F., & Quattrone, A. (2011). Altered cortical-cerebellar circuits during verbal working memory in essential tremor. *Brain*, *134*, 2274–2286.

Patel, A. X., Kundu, P., Rubinov, M., Jones, P. S., Vertes, P. E., Ersche, K. D., Suckling, J., & Bullmore, E. T. (2014). A wavelet method for modeling and despiking motion artifacts from resting-state fMRI time series. *NeuroImage*, *95*, 287–304.

Pereira, L., Airan, R. D., Fishman, A., Pillai, J. J., Kansal, K., Onyike, C. U., Prince, J. L., Ying, S. H., & Sair, H. I. J. H. B. M. (2017). Resting-state functional connectivity and cognitive dysfunction correlations in spinocerebelellar ataxia type 6 (SCA6). *Human Brain Mapping*, *6*(SCA6), 38–3010.

Piccinin, C. C., Rezende, T. J. R., de Paiva, J. L. R., Moyses, P. C., Martinez, A. R. M., Cendes, F., & Franca, M. C., Jr. (2020). A 5-year longitudinal clinical and magnetic resonance imaging study in spinocerebellar ataxia type 3. *Movement Disorders*, *35*, 1679–1684.

Power, J. D., Barnes, K. A., Snyder, A. Z., Schlaggar, B. L., & Petersen, S. E. (2013). Steps toward optimizing motion artifact removal in functional connectivity MRI; a reply to carp. *NeuroImage*, *76*, 439–441.

Reetz, K., Dogan, I., Rolfs, A., Binkofski, F., Schulz, J. B., Laird, A. R., Fox, P. T., & Eickhoff, S. B. (2012). Investigating function and connectivity of morphometric findings—Exemplified on cerebellar atrophy in spinocerebellar ataxia 17 (SCA17). *NeuroImage*, *62*, 1354–1366.

Rezende, T. J. R., de Paiva, J. L. R., Martinez, A. R. M., Lopes-Cendes, I., Pedroso, J. L., Barsottini, O. G. P., Cendes, F., & Franca, M. C., Jr. (2018). Structural signature of SCA3: From presymptomatic to late disease stages. *Annals of Neurology*, *84*, 401–408.

Rub, U., Schols, L., Paulson, H., Auburger, G., Kermer, P., Jen, J. C., Seidel, K., Korf, H. W., & Deller, T. (2013). Clinical features, neurogenetics and neuropathology of the polyglutamine spinocerebellar ataxias type 1, 2, 3, 6 and 7. *Progress in Neurobiology*, *104*, 38–66.

Saad, Z. S., Gotts, S. J., Murphy, K., Chen, G., Jo, H. J., Martin, A., & Cox, R. W. (2012). Trouble at rest: How correlation patterns and group differences become distorted after global signal regression. *Brain Connectivity*, *2*, 25–32.

Samson, M., & Claassen, D. O. (2017). Neurodegeneration and the cerebellum. *Neurodegenerative Diseases*, *17*, 155–165.

Stefanescu, M. R., Dohnalek, M., Maderwald, S., Thurling, M., Minnerop, M., Beck, A., Schlamann, M., Diedrichsen, J., Ladd, M. E., & Timmann, D. (2015). Structural and functional MRI abnormalities of cerebellar cortex and nuclei in SCA3, SCA6 and Friedreich's ataxia. *Brain*, *138*, 1182–1197.

Tzvi, E., Zimmermann, C., Bey, R., Munte, T. F., Nitschke, M., & Kramer, U. M. (2017). Cerebellar degeneration affects cortico-cortical connectivity in motor learning networks. *Neuroimage Clinical*, *16*, 66–78.

Vogel, J. W., La Joie, R., Grothe, M. J., Diaz-Papkovich, A., Doyle, A., Vachon-Presseau, E., Lepage, C., Vos de Wael, R., Thomas, R. A., Iturria-Medina, Y., & Bernhardt, B. (2020). A molecular gradient along the longitudinal axis of the human hippocampus informs large-scale behavioral systems. *Nature Communications*, *11*, 960.

Vos de Wael, R., Benkarim, O., Paquola, C., Lariviere, S., Royer, J., Tavakol, S., Xu, T., Hong, S. J., Langs, G., Valk, S., Misic, B., Milham, M., Margulies, D., Smallwood, J., & Bernhardt, B. C. (2020). BrainSpace: A toolbox for the analysis of macroscale gradients in neuroimaging and connectomics datasets. *Communications Biology*, *3*, 103.

Vos de Wael, R., Lariviere, S., Caldairou, B., Hong, S. J., Margulies, D. S., Jefferies, E., Bernasconi, A., Smallwood, J., Bernasconi, N., & Bernhardt, B. C. (2018). Anatomical and microstructural determinants of hippocampal subfield functional connectome embedding. *Proceedings of the National Academy of Sciences of the United States of America*, *115*, 10154–10159.

Wan, N., Chen, Z., Wan, L., Tang, B., & Jiang, H. (2020). MR Imaging of SCA3/MJD. *Frontiers in Neuroscience*, *14*, 749.

Wang, X. J. (2020). Macroscopic gradients of synaptic excitation and inhibition in the neocortex. *Nature Reviews. Neuroscience*, *21*, 169–178.

Witter, L., & De Zeeuw, C. I. (2015). Regional functionality of the cerebellum. *Current Opinion in Neurobiology*, *33*, 150–155.

Worbe, Y. (2015). Neuroimaging signature of neuropsychiatric disorders. *Current Opinion in Neurology*, *28*, 358–364.

Xu, K. B., Liu, Y., Zhan, Y. F., Ren, J. J., & Jiang, T. Z. (2018). BRANT: A versatile and extendable resting-state fMRI toolkit. *Frontiers in Neuroinformatics*, *12*, 13.

Yan, C. G., Cheung, B., Kelly, C., Colcombe, S., Craddock, R. C., Di Martino, A., Li, Q. Y., Zuo, X. N., Castellanos, F. X., & Milham, M. P. (2013). A comprehensive assessment of regional variation in the impact of head micromovements on functional connectomics. *NeuroImage*, *76*, 183–201.

Yan, C.-G., Wang, X.-D., Zuo, X.-N., & Zang, Y.-F. (2016). DPABI: Data Processing & Analysis for (resting-state) brain imaging. *Neuroinformatics*, *14*, 339–351.

Yap, K. H., Kessels, R. P. C., Azmin, S., van de Warrenburg, B., & Mohamed Ibrahim, N. (2022). Neurocognitive changes in spinocerebellar ataxia type 3: A systematic review with a narrative design. *Cerebellum*, *21*, 314–327.

Zhang, H., Ji, S., Ren, S., Liu, M., Ran, W., Zhang, X., Tian, W., Chen, Z., & Wang, Z. (2020). Cerebellar atrophy in multiple system atrophy (cerebellar type) and its implication for network connectivity. *Cerebellum*, *19*, 636–644.

Zhou, J., Gennatas, E. D., Kramer, J. H., Miller, B. L., & Seeley, W. W. (2012). Predicting regional neurodegeneration from the healthy brain functional connectome. *Neuron*, *73*, 1216–1227.

SUPPORTING INFORMATION

Additional supporting information can be found online in the Supporting Information section at the end of this article.

How to cite this article: Liu, X., Guo, J., Jiang, Z., Liu, X., Chen, H., Zhang, Y., Wang, J., Liu, C., Gao, Q., & Chen, H. (2024). Compressed cerebellar functional connectome hierarchy in spinocerebellar ataxia type 3. *Human Brain Mapping*, *45*(3), e26624. https://doi.org/10.1002/hbm.26624